Depression of the nematic-isotropic phase transition temperature at nanopatterned surfaces

Bing Wen,[1] Jong-Hyun Kim,[2] Hiroshi Yokoyama,[2,3] and Charles Rosenblatt[1,*]
[1]*Department of Physics, Case Western Reserve University, Cleveland, Ohio 44106-7079*
[2]*Yokoyama Nano-structured Liquid Crystal Project, ERATO, Japan Science and Technology Corporation, 5-9-9 Tokodai, Tsukuba, Ibaraki 300-2635, Japan*
[3]*Nanotechnology Research Institute, National Institute of Advanced Industrial Science and Technology, Tsukuba, Ibaraki 305-8568, Japan*
(Received 14 February 2002; published 21 October 2002)

A spatially varying herringbone pattern with an easy axis alternating in angle between 0 and ψ and having a period of 200 nm was scribed into a polyimide-coated substrate. The depression of the nematic-isotropic transition temperature for a nematic layer at the patterned surface relative to its value at a uniformly rubbed surface was investigated as a function of ψ for $15 < \psi < 88°$. It was found that the depression of the transition temperature increases with ψ, up to ≈ 7 mK at $\psi = 88°$. A simple model was developed that includes not only elasticity, but also anchoring effects at the polyimide. The model, which is used to calculate the thickness of the nematic layer, indicates that anchoring—rather than elastic—effects play the dominant role in the depression of the layer's transition temperature.

DOI: 10.1103/PhysRevE.66.041502 PACS number(s): 61.30.Gd, 64.70.Nd

About 12 years ago Barbero and Durand showed theoretically [1] that if the nematic liquid crystal director attempts to follow the topography of a rough surface, the cost of the associated curvature elastic energy may result in a decrease of the nematic order parameter S near the surface, or even in melting into the isotropic phase. This occurs because the curvature elastic moduli are functions of S: A decrease of the order parameter results in a decreased elastic energy cost. Several qualitative and semiquantitative experimental results for rough surfaces subsequently have been reported [2–7]. Yokoyama, Kobayashi, and Kamei, for example, observed a depression of the order parameter at the surface, which was attributed in part to surface roughness [2]. Additionally, they found an anomalous decrease of the anchoring strength near the nematic-isotropic phase transition due to curvature at the substrate and the resulting decrease of S [3]. Wu and Efron found that the optical phase retardation is not proportional to cell thickness when the surface is roughened with a sputtered SiO_2 layer [4]. They interpreted this result in terms of a reduced order parameter, and therefore a reduced optical birefringence, near the surfaces. Analogous results were obtained by Barberi and Durand [5]. Because the elastic melting model [1] was unable to fully explain their results, they invoked order electricity [8] in their analysis. More recently Papanek and Martinot-Lagarde used a surface plasmon technique to investigate order at a rough SiO_x surface [6]. They found that the difficult-to-purify liquid crystal methoxybenzylidene butylanaline that penetrates the voids has zero order parameter over the entire bulk nematic range, and that a continuous transition of the nematic order parameter S from near zero at the SiO_x surface to its bulk value in the central part of the cell occurs over a correlation length of several nanometers. Again, order electricity was invoked to explain the results. Monkade *et al.* examined the behavior of the liquid crystal at a surface covered with needles and columns of SiO and found that the roughness results in a decrease of the order parameter [7]. A model that minimizes the melting energy (as opposed to the elastic energy) and includes order electricity was needed to explain their full set of results.

With the advent of nanoscopic control of the surface by atomic force nanolithography [9], it has become possible to compel the liquid crystal director to adopt a well-defined profile that varies on very short length scales. This is accomplished by the use of the stylus of an atomic force microscope, whereby tiny patterns are scribed into the polymer that coats the substrate. Pixels as small as tens of nanometers are possible, with each pixel having a unique easy axis for director orientation. This technique has been used to create optical devices [9,10] and to examine the interaction between the liquid crystal and substrate [11,12]. Moreover, because atomic force nanolithography relies primarily on the inherent anchoring of a substrate that is patterned for planar alignment, it is considerably easier to control than the surface topography [4–7]. In consequence it is now possible to investigate in great detail the issue of the substrate's effect on nematic nucleation and melting.

In this paper we examine how substrate-imposed elastic deformations affect the nucleation temperature of a nematic layer at the substrate. We have created nanoscopic herringbone patterns in a polyimide-coated substrate, where each period λ contains two very long pixels, such that the easy axes of the two pixels form an angle ψ. The depression ΔT of the nematic layer's transition temperature *relative to its value at a uniformly oriented surface* was investigated as a function of ψ, where it was found that the magnitude of ΔT increases monotonically with ψ up to ≈ 7 mK at $\psi = 88°$. A model for the surface energy that includes not only elasticity, but anchoring effects at the polyimide interface, was used in conjunction with the Kelvin equation and the data for ΔT to determine the thickness of the nucleated nematic layer [13]. The calculation, which does not include order electricity, indicates that anchoring—rather than elastic—effects play the dominant role in the depression of the transition temperature.

Two indium-tin-oxide-coated glass substrates were cleaned sequentually in detergent, acetone, and ethanol. The

*Corresponding author. Email address: cxr@po.cwru.edu

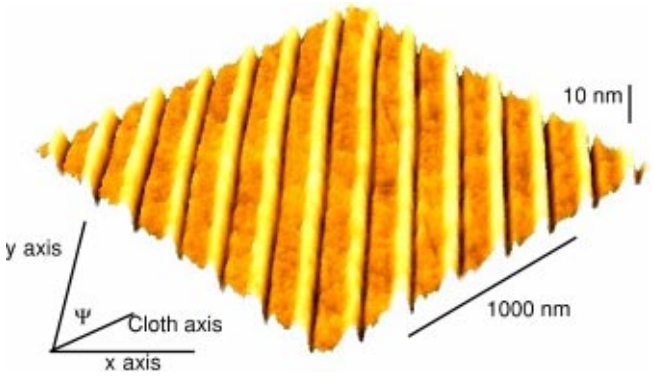

FIG. 1. AFM picture taken in noncontact mode of a section of the AFM-scribed square. In-plane and out-of-plane scales are shown. The raised sections correspond to the cloth-rubbed regions, and the recessed sections to regions that subsequently have been scribed by the AFM stylus. The *y* axis is parallel to the AFM-scribed lines, and the *x* axis is perpendicular. ψ is the angle between the AFM-scribed lines and the cloth-rubbed direction.

polyimide PI-2555 (DuPont) was spin coated on the substrates and cured at 275 °C for 2 h. A rubbing machine was then used to buff the substrates with a cotton cloth. One of the substrates then was scribed (over-rubbed) with an applied force of ≈ 5 μN over an area of 100 μm$\times$100 μm using the silicon stylus of a Topometrix atomic force microscope (AFM). The AFM-scribed lines were oriented at an angle of ψ with respect to the cloth-rubbing direction, and were ≈ 100 μm long and 100 nm in width. A gap of ≈ 100 nm was left between each AFM-scribed line, resulting in a period $\lambda \approx 200$ nm along the *x* axis. Choosing the *y* axis as the direction of the AFM-scribed lines, the result was a herringbone pattern of two easy axes, making angles of 0 and ψ, respectively, with respect to the *y* axis. An AFM image of a typical rubbed pattern is shown in Fig. 1. The long troughs correspond to the AFM-scribed regions, and are ≈ 4 nm deeper than the adjacent cloth-buffed regions. Note that the cross section of the topography is not quite square: As the AFM stylus scribes the polyimide, some of the polymer is pushed to the side, forming a ridge that runs alongside the trough. The width of the ridge is ≈ 25 nm, and its peak height above the adjacent cloth-buffed region is ≈ 4 nm. The AFM-scribed slide contained eight patterned squares, each having a different value of ψ for $15 \leqslant \psi \leqslant 88°$. The two substrates—one both cotton cloth rubbed and AFM scribed, and the other rubbed by the cotton cloth only—were then placed together, separated by Mylar spacers of nominal thickness *t*, and cemented. Three such cells were made having $t = 5$, 25, and 125 μm.

Each cell in turn was housed in an Instec temperature-controlled oven, which was placed on the stage of a polarizing optical microscope. The cell then was filled in the isotropic phase with the liquid crystal octyloxycyanobiphenyl (8OCB), supplied by Merck and used without further purification, and slowly cooled toward the nematic phase at a very slow rate of -4 mK min^{-1}. Because the nematic (rather than the isotropic) phase wets the polyimide-coated substrate [14] for *both* rubbing conditions, one ordinarily would expect a uniform nematic wetting layer to extend over a surface that is uniform in temperature and slightly above the bulk nematic-isotropic (NI) transition temperature T_{NI}. However, a temperature gradient was present, which varied from 30 to 60 mK mm^{-1} in the plane of the cell (depending upon the position). (Additionally, a small vertical temperature gradient also was present, such that the cell was arranged with the AFM-scribed square situated on the colder side of this vertical gradient). Thus, a well-defined nucleated nematic layer was observed to move across the cell with decreasing temperature. The nematic layer was very thin near the ''head'' of the front and increased in thickness toward the ''tail,'' which corresponds to the NI interface in the center region of the cell (see Fig. 2). To the right of the tail the cell is again monophasic. The distance between the head and tail depends upon the surface wetting characteristics and temperature gradients, and also may be influenced by impurities, whose concentration is tiny in this liquid crystalline material. Using a polarizing microscope and noting the optical transmission through the thin nematic region, we estimate the angle of the nematic layer to be $\beta \sim 0.002$ rad. It is important to remark that this region corresponds to the nucleated nematic phase, rather than the surface-induced paranematic order.

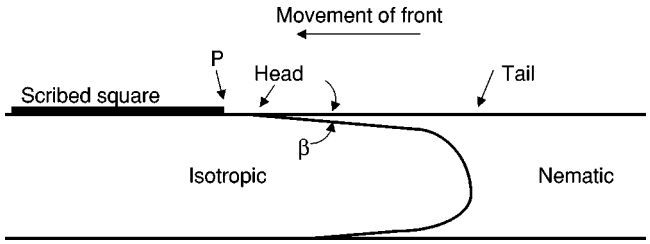

FIG. 2. Schematic diagram of cell cross section. Point *P* corresponds to the position at which the head of the nematic layer becomes pinned at temperature T_1. Near the head of the front the nematic layer has an average characteristic thickness *d*.

As the head of the nematic layer reached a given AFM-scribed square, it became pinned at the boundary between the uniformly cloth-rubbed, nematic-friendly surface region and the AFM-scribed, nematic-hostile region, as shown in Fig. 3. (We note that *nematic hostile* is a relative term. The nematic phase wets the polyimide-coated substrate, independent of the rubbing conditions. This is contrary to the picture in Ref. [1] in which the nematic order at a rough SiO sub-

FIG. 3. Sequence of polarized photomicrographs of the head and its trailing thin nematic layer invading the AFM-scribed square on cooling. (The tail remains outside the image). (a) Head becoming pinned at point *P*, corresponding to temperature T_1; the temperature gradient is shown. (b) Head continues to move around square. (c) Head begins to advance beyond point *P* into square at temperature T_2. (d) Head advances further into square. The 100 μm$\times$100 μm AFM-scribed square is outlined, indicating the length scale in the images.

strate is less than it is in bulk. The reason for this difference lies in the substrate materials, with the polyimide ''preferring'' the nematic phase. Analogous effects were observed by Yokoyama *et al.* [15], where they found the isotropic phase wetted SiO and the nematic phase wetted polyvinyl alcohol substrates). We define T_1 as the temperature at which the nematic layer, i.e., the head of the phase front, just reached the square at point P [Fig. 3(a)]. As the temperature continued to decrease, the nematic layer continued to advance *outside* the square, i.e., the nematic layer began to envelop the AFM-scribed square when viewed from above, but in the region beneath the square the liquid crystal remained in the isotropic phase [Fig. 3(b)]. Note that although the head of the front remained pinned at point P, the tail continued to advance during this time. However, neither the tail nor the other head (at the warmer substrate) penetrated the square region until the primary head began to advance beyond point P. Then at a temperature T_2 the head of the nematic layer began to move into the square, beyond P [Fig. 3(c)]. We define as $\Delta T \equiv T_1 - T_2$, the difference in transition temperatures between a region at the uniformly rubbed substrate and at the square that was AFM scribed for a rapidly spatially varying easy axis. We emphasize that our experiment involves a measurement of the temperature *difference* ΔT, *not* the absolute nucleation temperature. ΔT could be determined to within ≈ 0.5–1 mK. Small values of ΔT, which are associated with small values of ψ, indicate that any impurities present did not become trapped. Two additional points need to be made: First, several selected cells also were examined with cooling rates of -8 mK min^{-1} and -1 mK min^{-1}. No significant differences in ΔT were observed, which strongly suggests that our observed effect is not a kinetic phenomenon. Consistent with this observation is the fact that similar results were obtained on heating, whereby the isotropic phase invaded the AFM-scribed square at temperatures lower than it did in the surrounding cloth-rubbed region. Second, we also investigated an AFM-scribed square with a high density of lines. In this case the line density was sufficiently high to eliminate the regions originally rubbed by the cloth; in effect, the square had a uniform (rather than herringbone) easy axis pattern. It turns out that ΔT for this case was negligible, indicating that nonzero values of ΔT are due to the herringbone structure.

Figure 4 shows experimental values of ΔT vs ψ for the three cells. When the angle ψ between the easy axes was small, ΔT was nearly—but not quite—equal to zero. This is as expected because the energy cost in the nematic phase due to a weakly spatially varying director is small. Thus, the nematic phase forms relatively easily at the AFM-scribed square, allowing the phase front to advance. With increasing angle ψ between the easy axes, however, ΔT was found to increase. Owing to the stronger spatial variations of the director, the isotropic phase was stabilized at the substrate to lower temperatures, deterring the nematic phase from wetting the substrate and thereby keeping the phase front pinned. Notice that to within experimental error, the value of ΔT is independent of cell thickness t.

In order to understand the observed behavior, we introduce a simple description that includes only the most salient

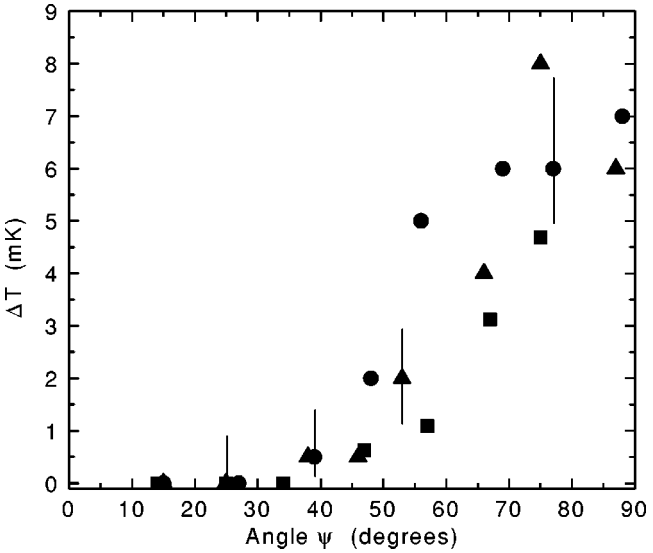

FIG. 4. Experimental values of $\Delta T_{\rm exp}$ vs ψ for cells of thickness $t=5$ (●), 25 (■), and 125 (▲) μm. Typical error bars are shown.

physical considerations. We emphasize that this paper is primarily experimental in nature and that the model is meant only to provide a basic understanding of the experimental results. Therefore, a number of relevant phenomena that quantitatively may affect the calculations have been omitted, and are discussed at the end. From the measurements of ΔT vs ψ our goal is to determine a characteristic average thickness d of the nematic layer near the head of the front.

We assume a simple picture of the front as shown in Fig. 2, viz., a very thin head region of thickness $\sim d$ behind which the nematic layer slowly becomes thicker with position. As the temperature is lowered, we make the approximation that the nematic layer thickness remains of order d at the head, but grows behind the head; this may be seen in Figs. 3(b) and 3(c). We begin the analysis with an effective surface energy density $F = F_w + F_k + F_m$ for a thin nematic layer at the substrate. The first term F_w corresponds to the anchoring energy and is composed of three parts: $F_w = F_{wi} + F_{wa} + F_{wp}$, where $F_{wi} = \frac{1}{2} W_i$ is the azimuthal orientation-independent part of the free energy per unit area—this is usually negative—that is associated with a nematic phase in contact with the polyimide substrate. It is primarily this term that causes the nematic phase to nucleate at the substrate, and is responsible for the small contact angle. The second component of F_w,

$$F_{wa} = \frac{1}{2} W_a \sin^2\theta \sin^2(\bar{\varphi} - \varphi), \tag{1}$$

is the azimuthal anchoring energy per area, and the third component

$$F_{wp} = \frac{1}{2} W_p \cos^2\theta \tag{2}$$

is the polar anchoring energy per unit area. W_a and W_p are the azimuthal and polar anchoring strength coefficients, respectively, φ and θ are the azimuthal and polar director ori-

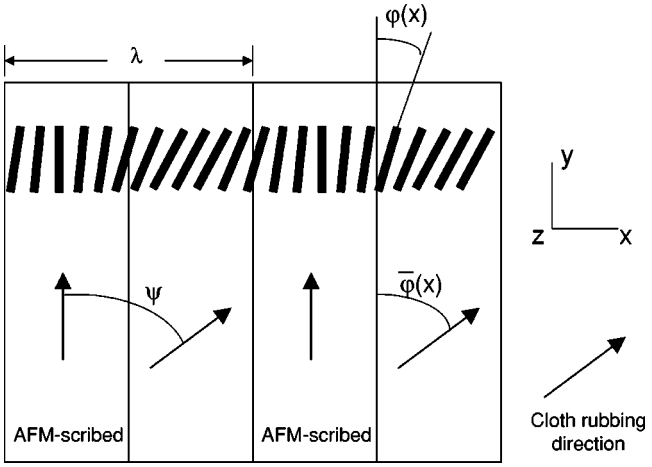

FIG. 5. Schematic representation of director pattern $\varphi(x)$ over two spatial periods λ. $\bar{\varphi}(x)$ is the easy axis pattern, and ψ is the angle between adjacent rubbing directions in one period.

entations and are functions of position x and z, and $\bar{\varphi}$ is the local azimuthal orientation of the easy axis (see Fig. 5). We remark that Eqs. (1) and (2) assume a periodic form in θ and φ, rather than the simpler Rapini-Papoular quadratic form [16]. At the uniformly cloth-rubbed surface the director lies along the easy axis and $F_w = F_{wi}$. At the AFM-scribed square, $\bar{\varphi} = 0$ in the pixel region $0 < x < \lambda/2$ and $\bar{\varphi} = \psi$ in the pixel region $\lambda/2 < x < \lambda$. For convenience it is assumed that the azimuthal anchoring strength coefficient W_a is identical in the cloth-rubbed and AFM-scribed regions, although our computer code allows for independent values. The same holds true for W_p and W_i. Before continuing, let us examine the relative importance of θ and φ. The anchoring energy F_w can be recast into the form

$$F_w = F_{wi} + \frac{1}{2}[W_a \sin^2(\bar{\varphi} - \varphi) + (W_p - W_a)\cos^2\theta \sin^2(\bar{\varphi} - \varphi) + W_p\{1 - \sin^2(\bar{\varphi} - \varphi)\}\cos^2\theta]. \quad (3)$$

Earlier we had obtained the anchoring strength coefficients at an AFM-scribed polyimide substrate, finding $W_a = 0.048$ and $W_p = 0.099$ erg cm^{-2} well into the nematic phase [17]. This is consistent with the fact that W_p is generally greater than W_a—in fact, often $W_p \gg W_a$ [18]. From Eq. (3) we see that each of the three terms in the integrand is positive definite, and that for a given value of $\bar{\varphi} - \varphi$, F_w is minimized for $\theta = \pi/2$, i.e., for planar alignment. Although elastic terms involving $\partial\theta/\partial x$ and $\partial\theta/\partial z$ may cause θ to deviate slightly from $\pi/2$, we shall see that the elastic energy $F_k \ll F_w$ and that any deviation from $\theta = \pi/2$ therefore must be small. Thus, because a transition to homeotropic alignment ($\theta = 0$) does not occur if $W_a < W_p$—and indeed, was not observed experimentally to occur—we shall take θ to be constant and equal to $\pi/2$; terms involving W_p therefore do not enter into the calculation.

The second term in F, i.e.,

$$F_k = \int \frac{1}{2}\sin^2\theta \left[k_1\left(\frac{\partial\varphi}{\partial x}\right)^2 + k_2\left(\frac{\partial\varphi}{\partial z}\right)^2\right] dz \quad (4)$$

corresponds to the elastic energy per unit area projected onto the surface, which is zero at the uniformly cloth-rubbed surface but is nonzero at the AFM-scribed surface region. Here k_1 is the splay elastic constant, which we approximate to be equal to the bend elastic constant [19], and k_2 is the twist elastic constant. The angle θ does not appear, as we have assumed it to be constant. The first term on the right hand side of Eq. (4) corresponds to a splay/bend elastic energy due to spatial variations of the projection of the director in the plane of the cell; the second term corresponds to the twist energy normal to the cell. The range of integration for z corresponds to the distance from the substrate into the bulk over which the director relaxes to a uniform azimuthal orientation; this distance is of order λ. We remark that the elastic energy associated with an average twist of the director due to nonparallel easy axes at the two opposing substrates is very small and can be neglected.

Beyond the substrate-nucleated nematic layer the nematic order parameter decays to zero over a distance of the order of the nematic correlation length ξ. The energy per unit area associated with this nematic - isotropic meniscus is

$$F_m \approx \frac{1}{2} D\xi\left(\frac{\partial S}{\partial z}\right)^2 \sec\beta, \quad (5)$$

where D, which is of the same order as the elastic constants, is the coefficient associated with order parameter gradients. The factor $\sec\beta$ indicates that the meniscus energy per unit area is projected onto the surface at the head of the front. F_m turns out to be of the same order of magnitude to a few times larger than F_{wa}. However, unlike F_{wa}, the meniscus term is present at *both* the cloth-rubbed and AFM-scribed regions. It thus contributes nearly equally to T_1 and T_2 because the angle $\beta \ll 1$ and is observed to increase by only a small amount (< 0.001 rad) when the head of the front invades the AFM-scribed square. As we are interested only in the *difference* $\Delta T = T_1 - T_2$, we shall ignore this term in the ensuing development, and take $F = F_w + F_k$.

In order to examine the effect of the herringbone pattern on the nematic-isotropic transition temperature, we need to estimate the nematic order parameter at the transition. As we are not aware of literature values for the Landua–de Gennes coefficients [19] for the liquid crystal 8OCB, we have have chosen to use values for a similar material, octylcyanobiphenyl [20]. On minimizing the Landau–de Gennes free energy, we find an order parameter $S = 0.294$ just inside the nematic phase.

For the splay elastic constant, Bradshaw *et al.* found $k_1 \sim 2 \times 10^{-7}$ dyn near the nematic-isotropic transition in 8OCB [21]. The twist elastic constant is normally about one-third the value of the splay constant [19]; thus, we use $k_2 = k_1/3$. The anchoring strength coefficient is more problematic. Sluckin and Poniewierski showed theoretically that the two leading terms in the expansion of the fundamental anchoring free energy scale linearly and quadratically with the value of the order parameter at the substrate [22]. In most

cases, however, the effective anchoring strength also may involve polar effects, flexoelectricity, and mobile charges. Indeed, several workers have found that the anchoring strength coefficient divided by S^2, where S is the bulk order parameter, is approximately constant well into the nematic phase [23,24], but decreases with decreasing S near the nematic-isotropic phase transition [3,23,25,26]. Based on these widely reported experimental results, we shall adopt the *ad hoc* empirical form $W_a = -G_a^o S + W_a^o S^2$, a form that simulates the temperature dependence of W_a reasonably well. Since $W_a = 0.048$ erg cm^{-2} deep in the nematic phase [17], we take $W_a^o = 0.12$ and $G_a^o = 0.02$ erg cm^{-2}. Because the temperature dependence of W_a for 8OCB at this substrate is not known, we have chosen these values for W_a^o and G_a^o to yield the correct value for W_a deep inside the nematic phase, and to show the correct qualitative decrease of W_a [3,23,25,26] near T_{NI}. Thus, at the transition where $S = 0.294$, these parameters yield an anchoring strength $W_a = 0.0045$ erg cm^{-2}. We have tested other reasonable combinations of W_a^o and G_a^o, and found that our final results are quantitatively similar.

The extrapolation length $L \equiv k_1 / W_a$ determines how well the director profile $\varphi(x, z=0)$ follows the scribed pattern $\overline{\varphi}(x)$ at the substrate, i.e., at $z=0$. We find that $L \sim 450$ nm at the transition, which is several times larger than the pixel size $\lambda/2$. If the pixels were larger than L, the director would align locally with the easy axes, except near the boundary between the pixels. However, since $L > \lambda/2$, the profile of φ is nearly sinusoidal in x with a period λ (Fig. 5). With $k_2 = k_1/3$ [19], the Euler-Lagrange equation can be applied to F_k in Eq. (4), resulting in a fundamental harmonic solution $\varphi(x,z) = \text{const} + \varphi_o \sin qx \exp(-\sqrt{3} qz)$, where $q = 2\pi/\lambda$. Although ultimately we will determine the x dependence of φ numerically, this solution shows that variations of φ along the substrate decay over a distance $z \sim \lambda/2\sqrt{3}\pi$ into the cell. Moreover, the associated elastic energy density decays over a distance $\lambda/4\sqrt{3}\pi$ into the cell. This is the relevant distance scale over which anchoring and elasticity contribute to the surface energy. Thus, F_k can be approximated in this region by replacing the integration over z in Eq. (4) with the multiplicative factor $\lambda/4\sqrt{3}\pi$ that corresponds to the decay length into the bulk of the elastic distortions. Therefore the energy per unit area $\overline{F}$ averaged over one period for a layer of thickness $\lambda/4\sqrt{3}\pi$ at the AFM-scribed substrate is given by

$$\overline{F} \equiv F_{wi} + \overline{F}_{wa} + \overline{F}_k = F_{wi} + \frac{1}{\lambda}\int_0^{\lambda} \left\{ W_a \sin^2(\overline{\varphi} - \varphi) + \frac{\lambda}{2\sqrt{3}\pi} k_1 \left(\frac{\partial \varphi}{\partial x} \right)_{z=0}^2 \right\} dx, \tag{6}$$

where φ is now a function of x only. (Note that $\overline{F} = F_{wi}$ at the uniformly cloth-rubbed surface). $\varphi(x)$ is determined numerically by dividing a full period λ into 100 units and minimizing $F_w + F_k$; peak-to-peak values $\varphi_{p\text{-}p}$ are shown in Fig. 6. From these values Eq. (6) may be used to determine the quantity $\overline{F} - F_{wi}$ $(= \overline{F}_{wa} + \overline{F}_k)$, which is shown in Fig. 7

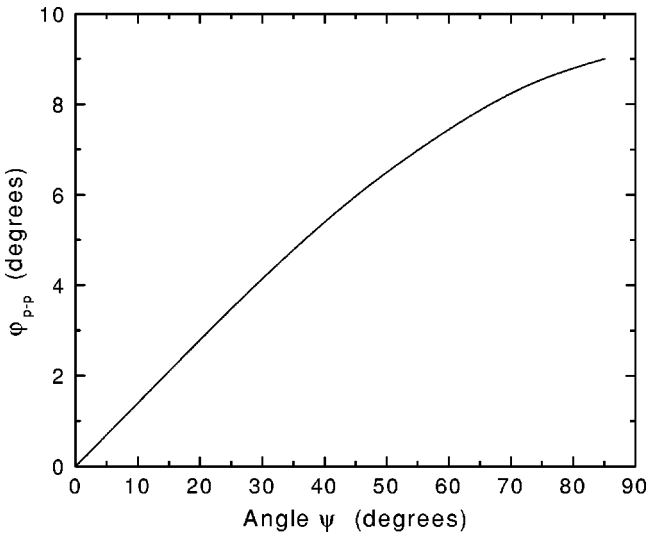

FIG. 6. Calculated peak-to-peak values $\varphi_{p\text{-}p}$ for $\varphi(x)$ vs ψ.

along with $\overline{F}_{wa}$ and $\overline{F}_k$ separately. It is clear from Fig. 7 that $\overline{F}_{wa}$ plays the dominant role in the overall surface energy. We note that because of the dominance of $\overline{F}_{wa}$, our approximation to ignore spatial variations of θ was reasonable.

Let us now turn to the Kelvin equation, which is a Clausius-Clapeyron-like equation for thin films [13]. The shift in transition temperature δT_j due to boundary effects can be expressed as

$$\delta T_j = \sum_{i=1,2} \frac{T_{NI}(F_i^N - F_i^I)_j}{Qd}, \tag{7}$$

where the subscript j refers to the AFM-scribed region (j = AFM) or uniformly cloth-rubbed region (j = CR). Q is the latent heat of the NI transition. Because the thin nematic layer has two boundaries (denoted by the subscript i), $i = 1$ refers to the boundary with the polyimide-coated substrate and $i = 2$ refers to the plane dividing the nematic layer with the bulk isotropic liquid crystal below. Finally, F_i^I and

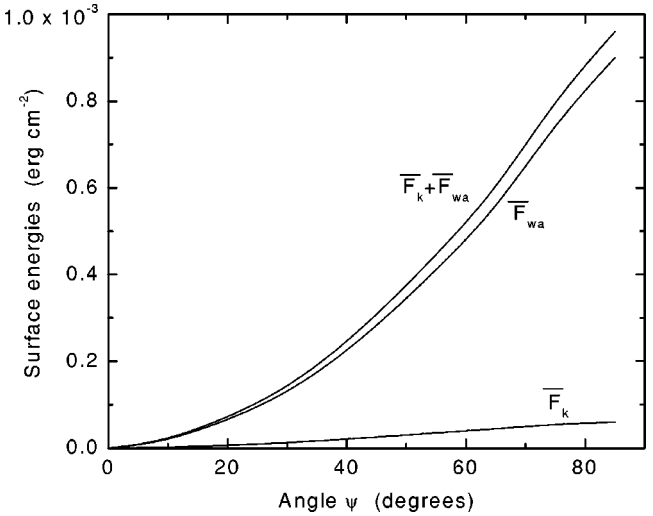

FIG. 7. Energies $\overline{F}_k$, $\overline{F}_{wa}$, and $\overline{F}_k + \overline{F}_{wa}$ vs ψ.

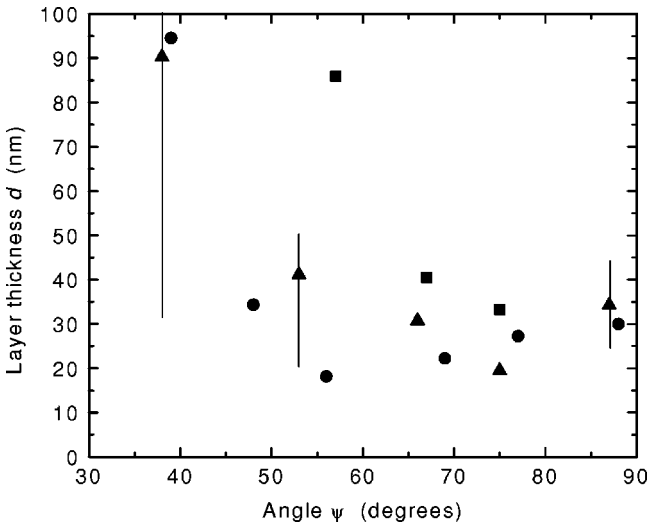

FIG. 8. Calculated characteristic nematic layer thickness d near the head of the front vs ψ for cells of thickness $d=5$ (●), 25 (■), and 125 (▲) μm. Because of the large relative uncertainty in measurements for ΔT at small angles, data are considered reliable only for $\psi \gtrsim 50°$.

F_i^N are the surface energies for the isotropic and nematic phases, respectively, in contact with boundary i. Our experiment measures $\Delta T \equiv \delta T_{j=\mathrm{AFM}} - \delta T_{j=\mathrm{CR}}$. By definition, $F_{i=2}^I$ is zero in both AFM-scribed ($j=$AFM) and cloth-rubbed ($j=$CR) regions, as this is just a continuation of an isotropic layer into the bulk. Additionally, $F_{i=2}^N$ corresponds to the nematic-isotropic meniscus energy discussed earlier, which we approximate as the same at both AFM-scribed and cloth-rubbed surfaces, and therefore cancels when calculating ΔT. Likewise, $F_{i=1}^I$ is the energy of the isotropic phase at the polyimide-coated ($i=1$) substrate, which is the same for both the AFM-scribed and cotton-cloth-rubbed regions for the approximations used herein; thus, these two terms cancel. The only nonzero and noncancelling terms involve $F_{i=1}^N$ for the $j=$AFM and $j=$CR regions, giving

$$\Delta T = \frac{T_{NI}(F_{i=1,j=AFM}^N - F_{i=1,j=CR}^N)}{Qd} = \frac{T_{NI}(\overline{F}_{wa} + \overline{F}_k)_{j=AFM}}{Qd}. \tag{8}$$

The transition temperature $T_{NI}=353$ K and, assuming a mass density of 0.981 g cm^{-3} [27], the latent heat $Q=1.76\times10^7$ erg cm^{-3} [28]. (Note that this is about two-thirds of the Landau–de Gennes value $Q=aS^2T_{NI}/2$ using appropriate values for a, b, and c). Using the experimental values for ΔT in Fig. 4 and the calculated values of $\overline{F}_{wa}+\overline{F}_k$ in Fig. 7, we calculate from Eq. (8) the average characteristic thickness d of the nematic layer near point P; the results are shown in Fig. 8 as a function ψ. Values for d at small ψ are unreliable owing mainly to the large relative uncertainty in measuring ΔT. As seen in Fig. 8, for larger ψ the data tend to scatter about a thickness $d\sim30$ nm. This is equal to about two nematic correlation lengths ξ, where ξ is typically about 15 nm near T_{NI} [29], as well as approximately twice the penetration depth of the elastic distortion $\lambda/2\pi\sqrt{3}$. We point out that the error bars in Fig. 8 represent uncertainty in the ΔT measurements. Additionally, the values for d may need to be scaled up or down due to the uncertainty in a, b, c, and W_a. We remark that although the calculated thickness d of the nematic layer does not depend strongly on k_1 alone, it *does* depend moderately strongly on the ratio k_2/k_1 because this ratio determines the thickness of the elastically deformed region [cf. Eq. (6)].

Despite the apparent reasonable values obtained for d, our procedure has a number of shortcomings. First, we assumed that S is spatially uniform in the elastically distorted interfacial region, and has a value equal to the bulk value at T_{NI}. Because this region is comparable in thickness to that of the nematic-isotropic meniscus, the order parameter S is likely to vary somewhat with z in this region. The result likely would be to reduce the calculated values $\overline{F}_k$, as the elastic energy cost would be smaller in regions of smaller S, i.e., away from the surface. (Interestingly, in principle S may even vary with x, i.e., it may be smaller in regions where the anchoring energy cost is large, and larger in other regions). Second, with decreasing temperature the nematic layer grows in thickness behind the front. A result of this growth is an increase in the angle β very close to the head; this would necessitate the inclusion of a component of meniscus energy in the calculation. Although the secβ factor keeps this contribution small, ultimately it may have a noticeable influence on our calculation for d. A third, related effect is that the model does not account explicitly for order electricity. Barbero and Durand calculated the effects of order electricity due to a gradient of the order parameter at a nematic– isotropic interface, finding that the equivalent energy per unit area is $\approx5\times10^{-3}$ ergs cm^{-2} [8]. Faetti and Palleschi have measured this quantity, obtaining smaller values of (1–2) $\times10^{-3}$ ergs cm^{-2} [30,31]. These values apparently are smaller than the anchoring strength coefficients used in our calculations. If the order electricity associated with a nematic-isotropic interface had been included in our effective surface energy $\overline{F}$, its effect would have been to stabilize the isotropic phase at *both* the AFM-scribed square and in the uniformly rubbed region in order to achieve a uniform phase throughout. In consequence our calculated values of d would have been little changed. Fourth, the model neglects surface-induced paranematic order in the bulk isotropic phase. This order would have been larger at the uniformly cloth-rubbed surface, slightly driving up T_1 and thereby increasing ΔT. Nevertheless, due to the weak paranematic order for our system, this correction is small compared to the observed results for ΔT.

Several other approximations also need to be mentioned. Our computational results assume that the anchoring strength coefficients are the same at both the cloth-rubbed and AFM-scribed substrates. However, if the coefficients at the two locations were to differ from each other by up to a factor of 2 (but with the same average value as above), we find that d would differ slightly—but not significantly—from our calculated values. Additionally, throughout our calculation we have ignored the elastic energy associated with a twist distortion from one surface of the cell to the other, or even the

possibility of nonzero θ at the meniscus. The former is of very long wavelength, and it has virtually no impact on our results; the latter may change our calculated value of $\overline{F_k}$ by up to 50%, but as this is small relative to $\overline{F_w}$, it would not have a great impact on our results. Finally, we note that on symmetry grounds flexoelectricity [32] does not play a role.

Control of the director profile on very short length scales opens up an exciting vista for the science and technology of liquid crystals. In this paper we demonstrated in a controlled manner the depression of the nematic-isotropic transition temperature, relative to its value for uniform orientation, by high energy, short length scale distortions and the associated anchoring energy. Unlike previous results, our modeling indicates that the dominant effect is due to anchoring at substrates that are wetted easily by the nematic phase, although order electricity may play an important—yet not prevailing—role. For future work it would be interesting to investigate systematically the role of impurities, as the nematic-isotropic equilibrium may affect the thickness of the nematic layer. Additionally, changing the nature of the polyimide would change the wetting angle, and therefore the thickness of the nematic layer at point *P*.

The authors have benefited from conversations with Professor T. J. Sluckin, Professor Rolfe G. Petschek, and Professor Philip L. Taylor. This work was supported by the U.S. Department of Energy's Office of Basic Energy Science under Grant No. DE-FG02-01ER45934.

[1] G. Barbero and G. Durand, J. Phys. II **1**, 651 (1991).
[2] H. Yokoyama, S. Kobayashi, and H. Kamei, J. Appl. Phys. **56**, 2645 (1984).
[3] H. Yokoyama, S. Kobayashi, and H. Kamei, J. Appl. Phys. **61**, 4501 (1987).
[4] S.-T. Wu and U. Efron, Appl. Phys. Lett. **48**, 624 (1986).
[5] R. Barberi and G. Durand, Phys. Rev. A **41**, 2207 (1990).
[6] J. Papanek and Ph. Martinot-Lagarde, J. Phys. II **6**, 205 (1996).
[7] M. Monkade, Ph. Martinot-Lagarde, G. Durand, and C. Grandjean, J. Phys. II **7**, 1577 (1997).
[8] G. Barebro, I. Dozov, J. F. Palierne, and G. Durand, Phys. Rev. Lett. **56**, 2056 (1986).
[9] M. Rüetschi, P. Grütter, J. Fünfschilling, and H.-J. Güntherodt, Science **265**, 512 (1994).
[10] Bing Wen, M. P. Mahajan, and C. Rosenblatt, Appl. Phys. Lett. **76**, 1240 (2000).
[11] J. H. Kim, M. Yoneya, J. Yamamoto, and H. Yokoyama, Appl. Phys. Lett. **78**, 3055 (2001).
[12] G. P. Sinha, C. Rosenblatt, and L. V. Mirantsev, Phys. Rev. E **65**, 041718 (2002).
[13] T. J. Sluckin and A. Poniewierski, Mol. Cryst. Liq. Cryst. **179**, 349 (1990).
[14] H. Yokoyama, S. Kobayashi, and H. Kamei, Appl. Phys. Lett. **41**, 438 (1982).
[15] H. Yokoyama, S. Kobayashi, and H. Kamei, Mol. Cryst. Liq. Cryst. **99**, 39 (1983).
[16] A. Rapini and M. Papoular, J. Phys. (Paris), Colloq. **30**, C4-54 (1969).
[17] Bing Wen and C. Rosenblatt, J. Appl. Phys. **89**, 4747 (2001).
[18] B. Jérôme, Rep. Prog. Phys. **54**, 391 (1991).
[19] P. G. de Gennes and J. Prost, *The Physics of Liquid Crystals* (Clarendon, Oxford, 1994).
[20] H. J. Coles, Mol. Cryst. Liq. Cryst. Lett. **49**, 67 (1978).
[21] M. J. Bradshaw, E. P. Raynes, J. D. Bunning, and T. E. Faber, J. Phys. (France) **46**, 1513 (1985).
[22] T. J. Sluckin and A. Poniewierski, in *Fluid Interfacial Phenomena*, edited by C. A. Croxton (Wiley, London, 1986).
[23] C. Rosenblatt, J. Phys. (France) **45**, 1087 (1984).
[24] Z. Zhuang, L. Marrucci, and Y. R. Shen, Phys. Rev. Lett. **73**, 1513 (1994).
[25] S. Faetti, M. Gatti, V. Palleschi, and T. J. Sluckin, Phys. Rev. Lett. **55**, 1681 (1985).
[26] J.-B. Fournier and P. Galatola, Phys. Rev. Lett. **82**, 4859 (1999).
[27] S. Sen, P. Brahma, S. K. Roy, D. K. Mukherjee, and S. B. Roy, Mol. Cryst. Liq. Cryst. **100**, 327 (1983).
[28] R. J. Cox, E. M. Barrall, A. Doelman, N. J. Clecak, J. A. Logan, R. D. Diller, and A. R. Gregges, Anal. Calorim. **4**, 37 (1977).
[29] B. P. Huff, J. J. Krich, and P. J. Collings, Phys. Rev. E **61**, 5372 (2000).
[30] S. Faetti and V. Palleschi, Phys. Rev. A **30**, 3241 (1984).
[31] S. Faetti and V. Palleschi, J. Phys. (France) Lett. **45**, 313 (1984).
[32] R. B. Meyer, Phys. Rev. Lett. **22**, 918 (1969).